Supporting Information

Solvent dependent formation of three new Bi-MOFs using a tetracarboxylic acid

Milan Köppen,[†] Vanessa Meyer,[†] Jonas Ångström,[‡] A. Ken Inge*,[‡] and Norbert Stock*,[†]

[†] M. Köppen, V. Meyer, Prof. Dr. N. Stock
Institut für Anorganische Chemie
Christian-Albrechts-Universität zu Kiel
Max-Eyth Str. 2, 24118 Kiel (Germany)
E-mail: stock@ac.uni-kiel.de

[‡] Dr. A. K. Inge, Dr. J. Ångström
Department of Materials and Environmental Chemistry
Stockholm University, Stockholm SE-106 91 (Sweden)

* correspondence to:

stock@ac.uni-kiel.de

andrew.inge@mmk.su.se

Table of Contents

1. Synthesis

The optimized synthesis conditions of CAU-31-33 can found in the experimental section of the article. The table of starting materials in the high-throughput reaction (manuscript Fig. 2) is shown in Table S1.

Table S1: Starting materials used in high-throughput reactions in a multiclave with 2 mL PTFE liners. The reactions were performed four times with heating for 1 h to target temperature (T), holding T for 12 h, and ramp down to room temperature for 1 h (with T = 80 °C, 100 °C, 120 °C, 140 °C).

molar ratio					
linker	metal	H_4TCPB / mg	$Bi(NO_3)_3 \cdot H_2O$ / mg	Solvent 1	Solvent 2
1	1	5.0	4.3	1000 µl MeOH	
1	2	5.0	8.7	1000 µl MeOH	
1	1	5.0	4.3	800 µl MeOH	200 µl DMF
1	2	5.0	8.7	800 µl MeOH	200 µl DMF
1	1	5.0	4.3	900 µl DMF	100 µl toluene
1	2	5.0	8.7	900 µl DMF	100 µl toluene

2. Scanning electron microscopy (SEM)

The SEM micrographs of CAU-31-33 are shown in Fig. S1.

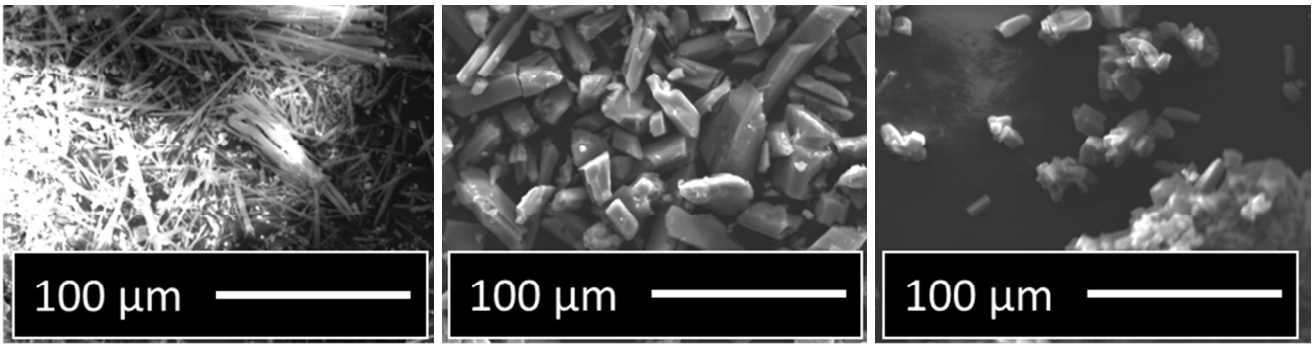

Fig. S1: SEM micrographs of CAU-31 (left), CAU-32 (*as*, middle) and *β*-CAU-33 (right).

3. Crystallographic information

3.1. CAU-31

Structure refinement was performed in TOPAS Academic 6[1] on a PXRD pattern in a range of 2 to 70° 2θ using the Rietveld method. Both crystallographically independent TCPB linkers were located on an inversion center and described using z-matrices, with the possibility to rotate the carboxylate groups and phenyl rings. Bond lengths inside the rigid body were each refined with one parameter, such as the $C_{phenyl}C_{phenyl}$-distance. The structural starting model for the Rietveld refinement was obtained from continuous rotation electron diffraction data (Fig. S2). Continuous rotation electron diffraction[2] datasets were collected on a high-speed hybrid-detection camera (Timepix Quad) in a JEOL JEM-2100 electron microscope with a LaB_6 source (λ = 0.0251 Å) in video mode from 12 crystals on lacey carbon on a copper grid using a cryo holder at -110 °C. Approximate lattice parameters and the space group were determined using REDp,[3] after which data reduction was performed in XDS.[4] The structure was successfully solved using dataset 4 (with a goniometer tilt from -40° to 58°, reduced from 879 images with an exposure time of 0.25 s, a completeness of 0.58 and R_{int} of 0.097) in ShelXT.[5] The crystallographic data is given in Table S2 based on the Rietveld refinement (Fig. S3).

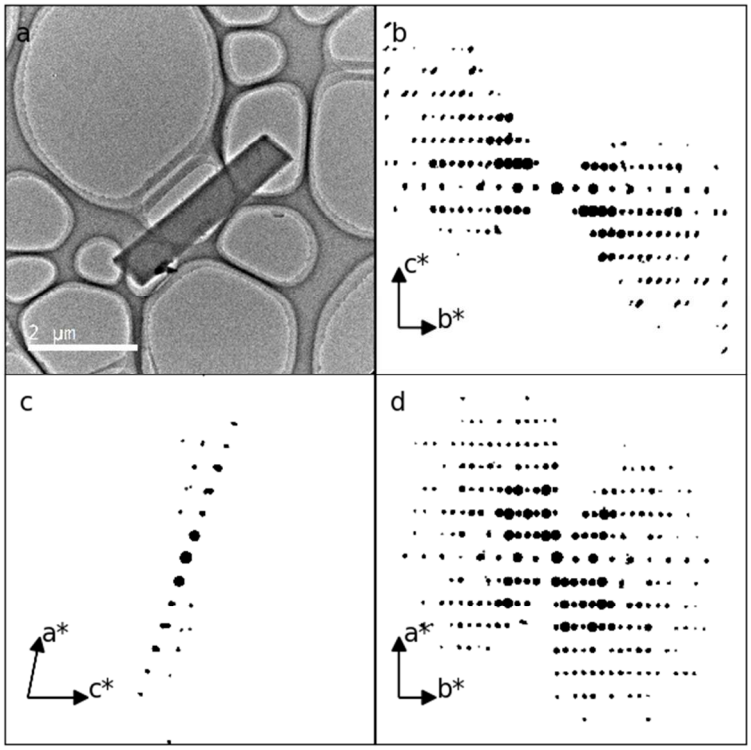

Fig. S2: TEM micrograph (a) and slices of the reconstructed reciprocal space (b, c, d) of CAU-31. Slices show (b) 0kl, (c) h0l and (d) hk0. The only obvious reflection condition is k=2n in 0kl and hk0. Information about conditions on l is lacking and some of the reflections seem to overlap.

Table S2: Crystallographic data and Rietveld refinement details on $[Bi_2(H_2TCPB)(TCPB)(H_2O)_2]\cdot xH_2O$ (CAU-31).

Identification code	CAU-31
Crystal system	Monoclinic
Space group	$P2_1/c$
Unit cell dimensions	a = 11.5261(5) Å
	b = 28.265(2) Å
	c = 11.575(2) Å
	β = 104.647(7)°
Volume	3648.4(5) Å^3
2Theta range for data collection	2 to 70°
Wavelength	1.5406 Å
Refinement method	Rietveld
R_{wp}	8.64 %
R_{exp}	2.26 %
GoF	3.81

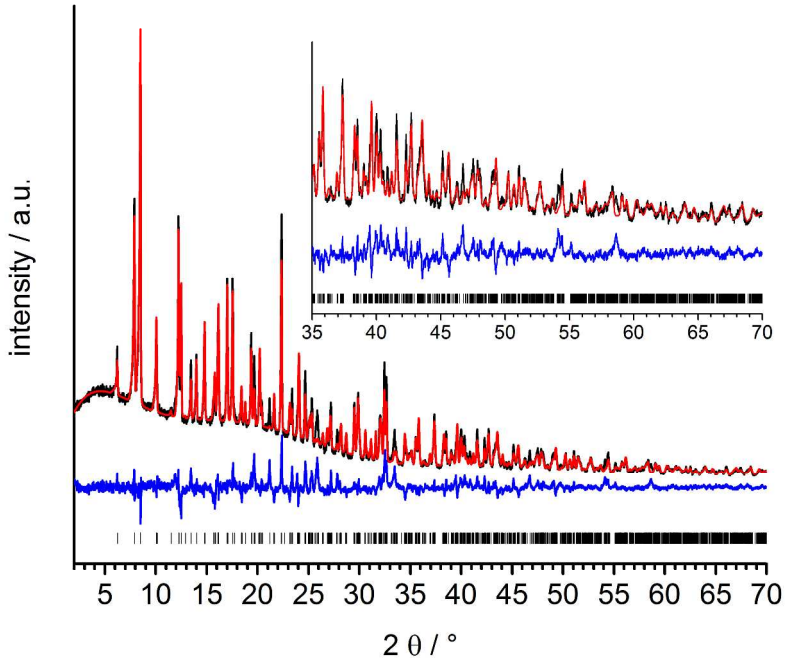

Fig. S3: Rietveld plot of the refinement of $[Bi_2(H_2TCPB)(TCPB)(H_2O)_2]\cdot xH_2O$ (CAU-31). Experimental and theoretical PXRD pattern shown as black and red line, respectively. The difference is drawn in blue, while the positions of the allowed reflections are indicated by black bars. The small deviations between observed and calculated intensities are probably due to the mobile guest molecules in the pores which were modelled as oxygen atoms.

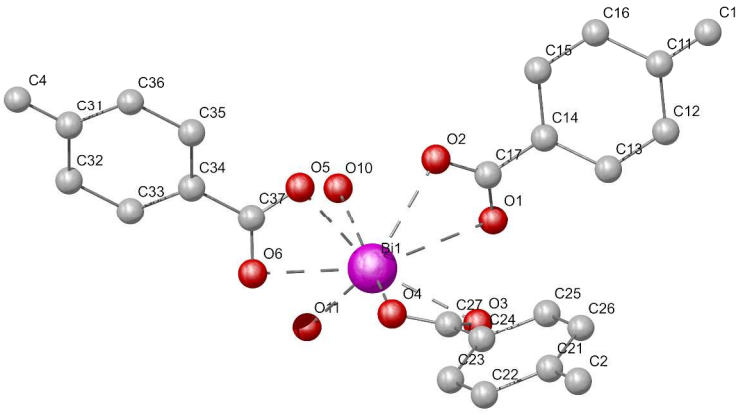

Fig. S4: Coordination sphere around the Bi^{3+} ion in CAU-31.

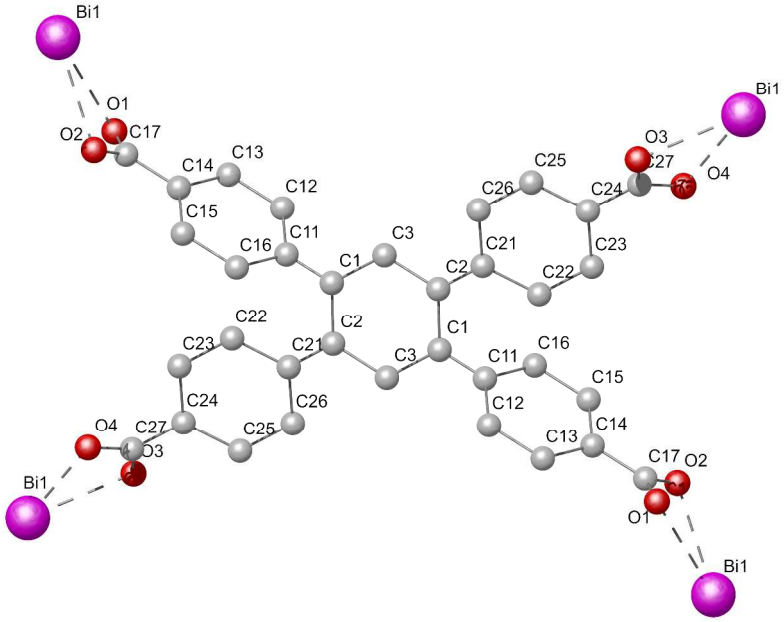

Fig. S5: Connection of Bi^{3+} ions by one $TCPB^{4-}$ ion in CAU-31.

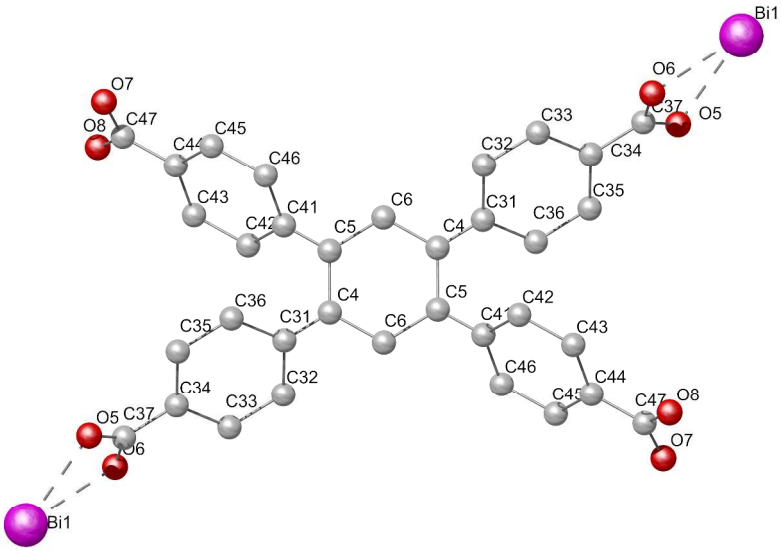

Fig. S6: Connection of Bi^{3+} ions by one H_2TCPB^{2-} ion in CAU-31.

3.2. CAU-32

A detailed description of the crystal structure determination is provided in the experimental section of the article. The crystallographic data and refinement details on CAU-32 (*as*) are presented in Table S3.

Table S3: Crystallographic data and refinement details on $(NH_2(CH_3)_2)[Bi(TCPB)(H_2O)]$ (CAU-32 (*as*)).

Identification code	CAU-32
Empirical formula	$C_{17}\ H_9\ Bi_{0.5}\ O_{4.5}$
Formula weight	389.73
Temperature	295(2) K
Wavelength	0.71073 Å
Crystal system	Monoclinic
Space group	$P2_1/n$
Unit cell dimensions	a = 11.188(1) Å
	b = 24.552(2) Å
	c = 16.315(2) Å
	β = 91.365(3)°
Volume	4480.1(8) $Å^3$
Z	8
Density (calculated)	1.156 g/cm^3
Absorption coefficient	3.973 mm^{-1}
F(000)	1508
Crystal size	0.12 x 0.07 x 0.05 mm^3
Theta range for data collection	2.232 to 26.492°
Index ranges	-14<=h<=13, -30<=k<=30, -20<=l<=20
Reflections collected	121023
Independent reflections	9210 [R(int) = 0.1756]
Completeness to theta = 25.242°	99.9 %
Absorption correction	Multi-scan
Max. and min. transmission	0.7454 and 0.6211
Refinement method	Full-matrix least-squares on F^2
Data / restraints / parameters	9210 / 6 / 397
Goodness-of-fit on F^2	1.052
Final R indices [I>2sigma(I)]	$R1$ = 0.0716, w$R2$ = 0.1328
R indices (all data)	$R1$ = 0.1274, w$R2$ = 0.1499
Largest diff. peak and hole	1.291 and -1.244 e/$Å^3$

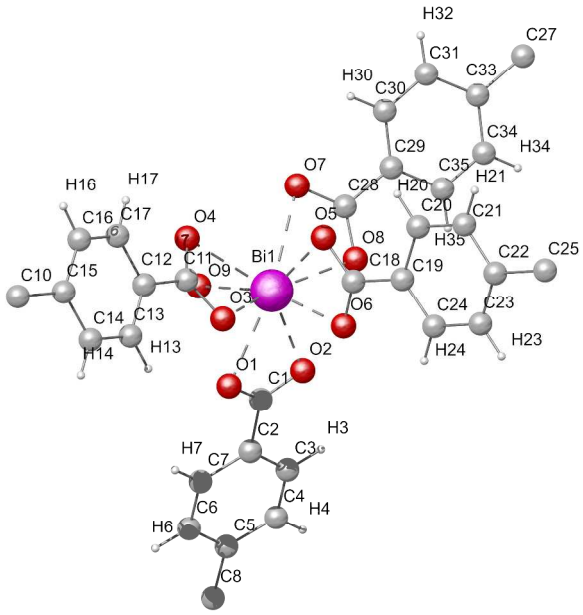

Fig. S7: Coordination sphere around the Bi^{3+} ion in CAU-32.

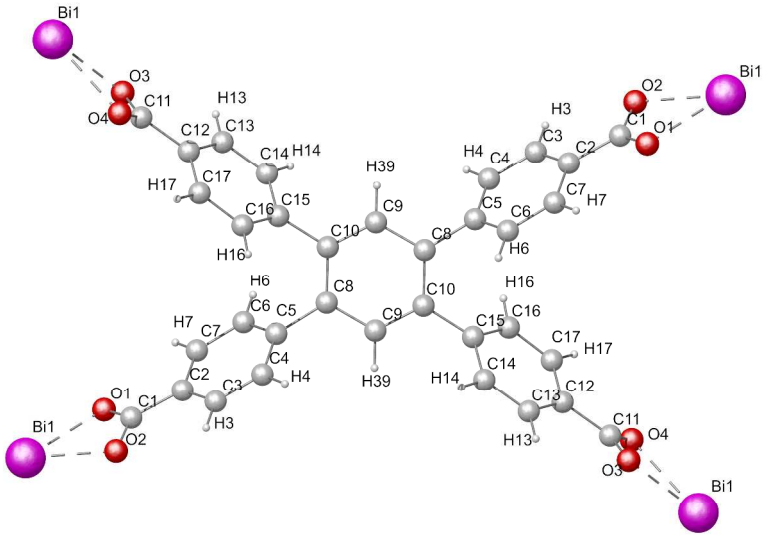

Fig. S8: Connection of Bi^{3+} ions by the $TCPB^{4-}$ ion in CAU-32.

3.3. *β*-CAU-33

The structure refinement was performed in TOPAS Academic 6[1] on a PXRD pattern in a range of 2 to 70° 2θ using the Rietveld method. Since both of the crystallographically independent TCPB-linkers lie on inversion centers, half of each linker was described using z-matrices, with the possibility to rotate the carboxylate groups and phenyl rings. Bond lengths inside the rigid body were each refined with one parameter, e.g. the $C_{phenyl}C_{phenyl}$-distance. The initial structural model was obtained by single-crystal X-ray diffraction (SC-XRD) including positions of the Bi cations and the approximate positions of the organic linker molecules. However due to the small crystal size (150 x 30 x 30 µm), overall the reflections were weak and the overall data quality was poor. Therefore, the structure was refined against X-ray powder diffraction data instead. The crystallographic data are provided in Table S4, the Rietveld plot in Fig. S9.

Table S4: Crystallographic data and Rietveld refinement details on $[Bi_4(O)_2(OH)_2(H_2TCPB)(TCPB)(H_2O)_2]\cdot xH_2O$ (*β*-CAU-33).

Identification code	*β*-CAU-33
Crystal system	Monoclinic
Space group	*C*2/*c*
Unit cell dimensions	*a* = 33.001(2) Å
	b = 22.909(2) Å
	c = 10.435(1) Å
	β = 99.53(1)°
Volume	7779.9(2) Å^3
2Theta range for data collection	2 to 70°
Refinement method	Rietveld
Wavelength	1.5406 Å
R_{wp}	4.29 %
R_{exp}	0.66 %
GoF	6.47

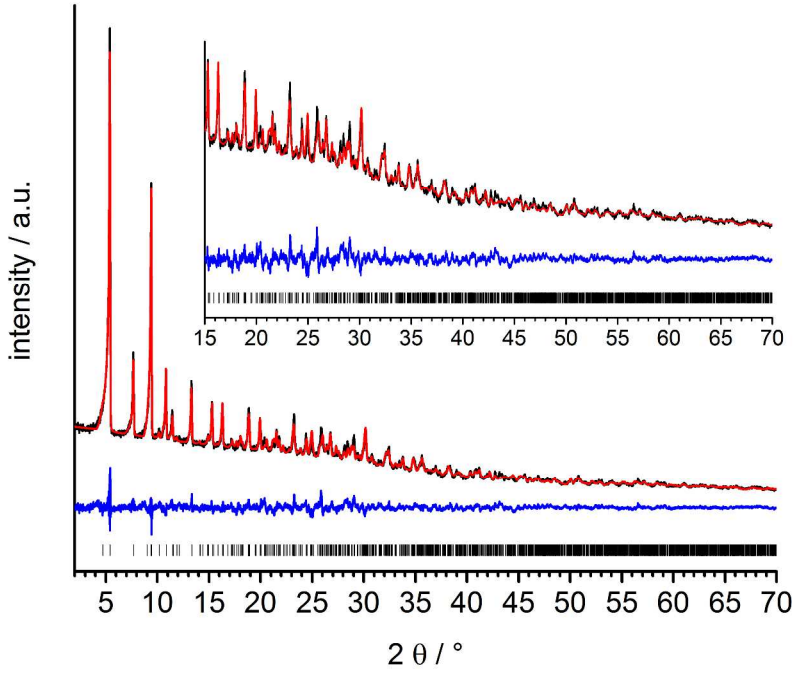

Fig. S9: Rietveld plot of the refinement of $[Bi_4(O)_2(OH)_2(H_2TCPB)(TCPB)(H_2O)_2]\cdot xH_2O$ (β-CAU-33). Experimental and theoretical PXRD pattern shown as black and red line, respectively. The difference is drawn in blue, while the positions of the allowed reflections are indicated by black bars.

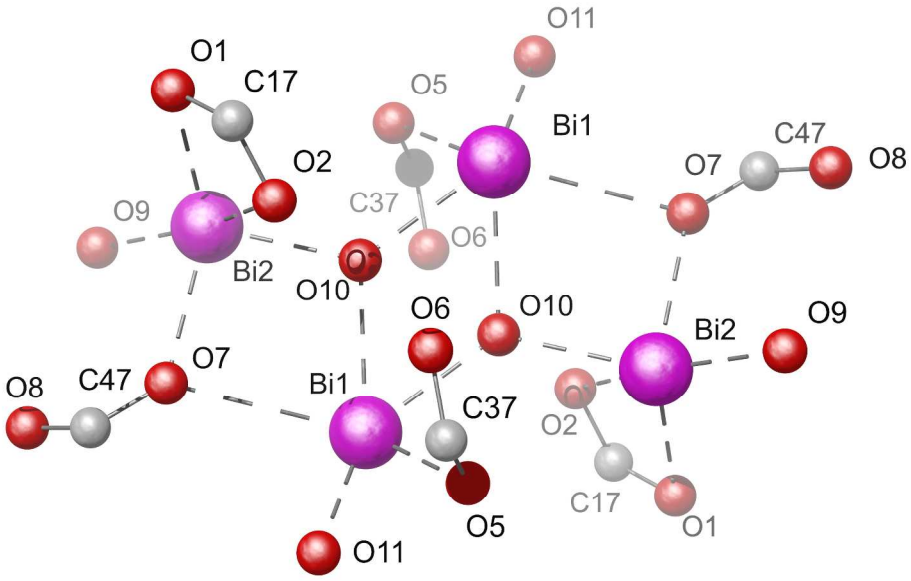

Fig. S10: Coordination sphere around the two symmetry independent Bi^{3+} ions in β-CAU-33.

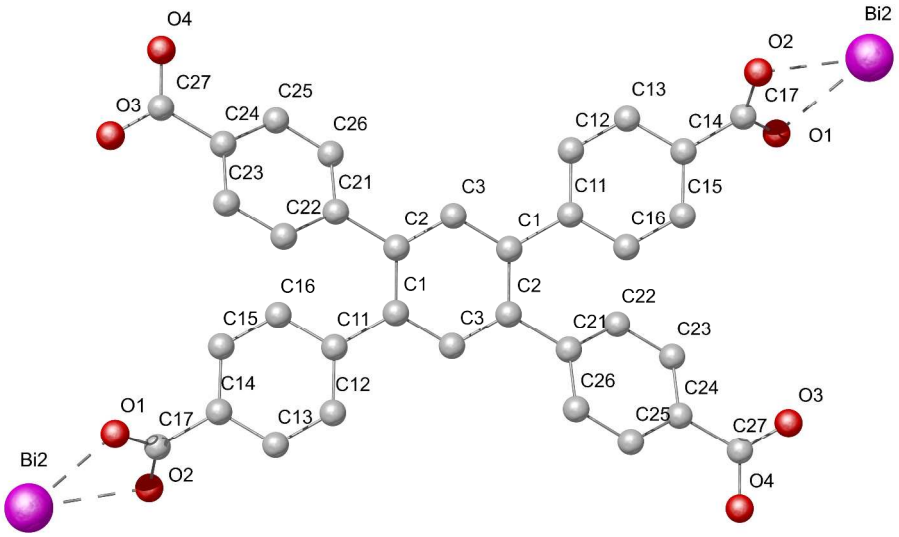

Fig. S11: Connection of Bi^{3+} ions by one H_2TCPB^{2-} ion in *β*-CAU-33.

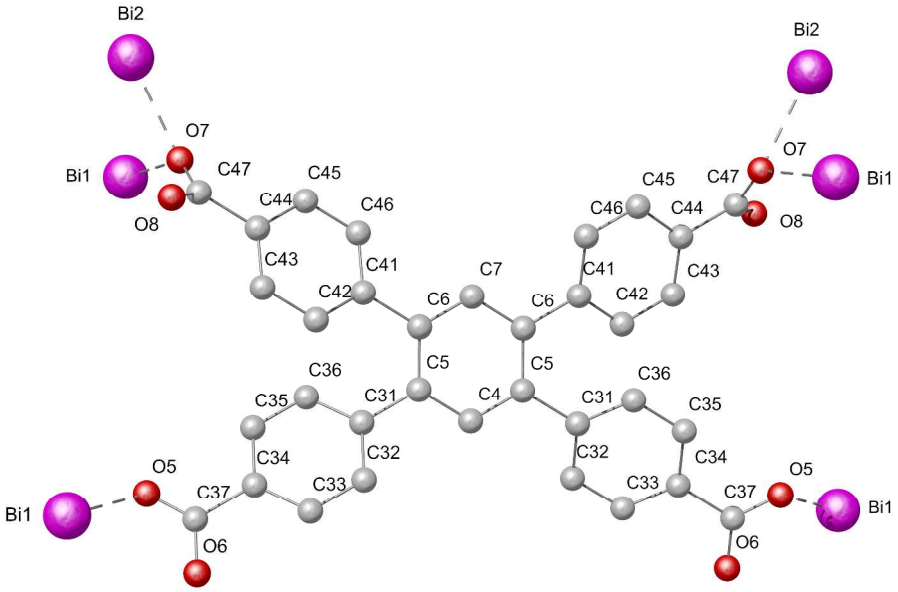

Fig. S12: Connection of Bi^{3+} ions by one $TCPB^{4-}$ ion in *β*-CAU-33.

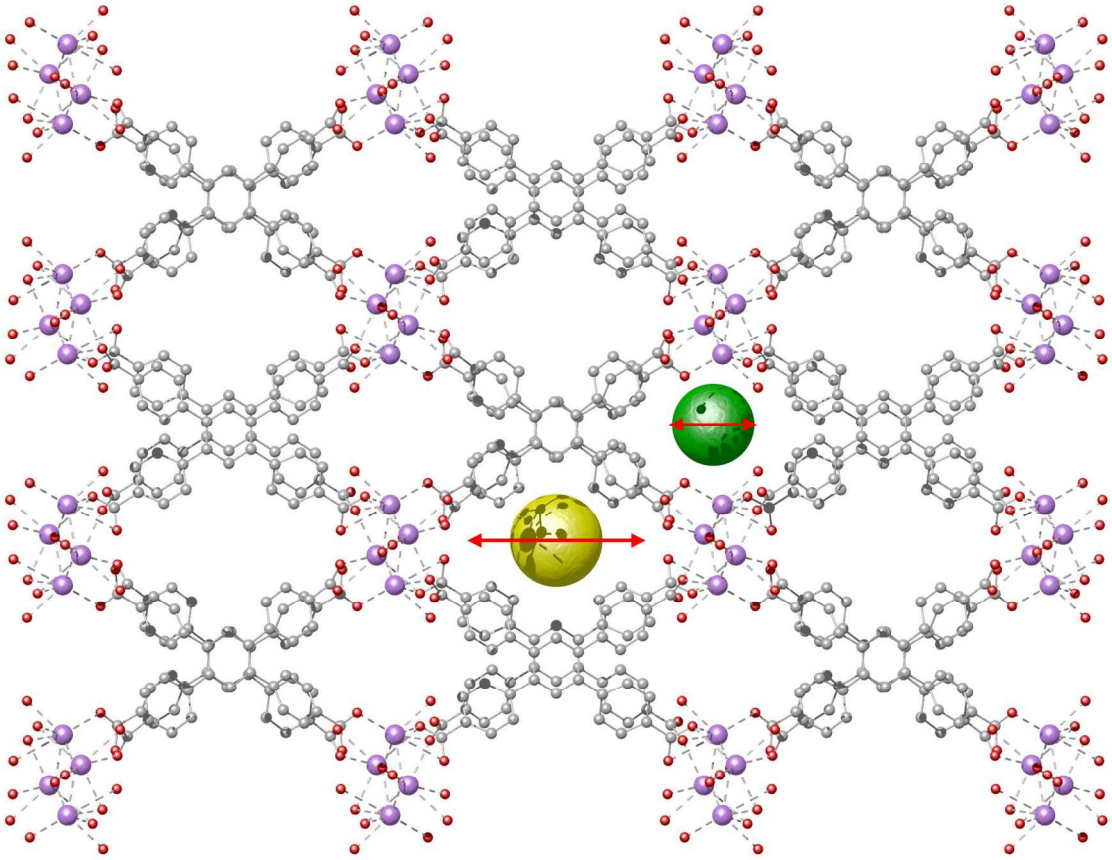

Fig. S13: Visualization of the two 1D lozenge-shaped channels in yellow and green in the crystal structure of *β*-CAU-33. The red arrows illustrate the dimension of the channels along [100] with 9.5×4.6 Å and 4.4×4.1 Å taking the van der Waals radii of framework atoms into account. View along [001].

3.4. *α*-CAU-33

The Le Bail fit (Fig. S14) was performed in TOPAS Academic 6[1] on a PXRD pattern in a range of 2 to 45° 2θ. The fit details are given in Table S5.

Table S5: Le Bail fit details on *α*-CAU-33.

Identification code	*α*-CAU-33
Crystal system	Monoclinic
Space group	*C*2/*c*
Unit cell dimensions	*a* = 32.785(4) Å
	b = 23.011(4) Å
	c = 10.139(2) Å
	β = 110.74(1)°
Volume	7153.63 Å^3
2Theta range for data collection	2 to 45°
Wavelength	1.5406 Å
Refinement method	Le Bail
R_{wp}	11.39 %
R_{exp}	6.49 %
GoF	1.76

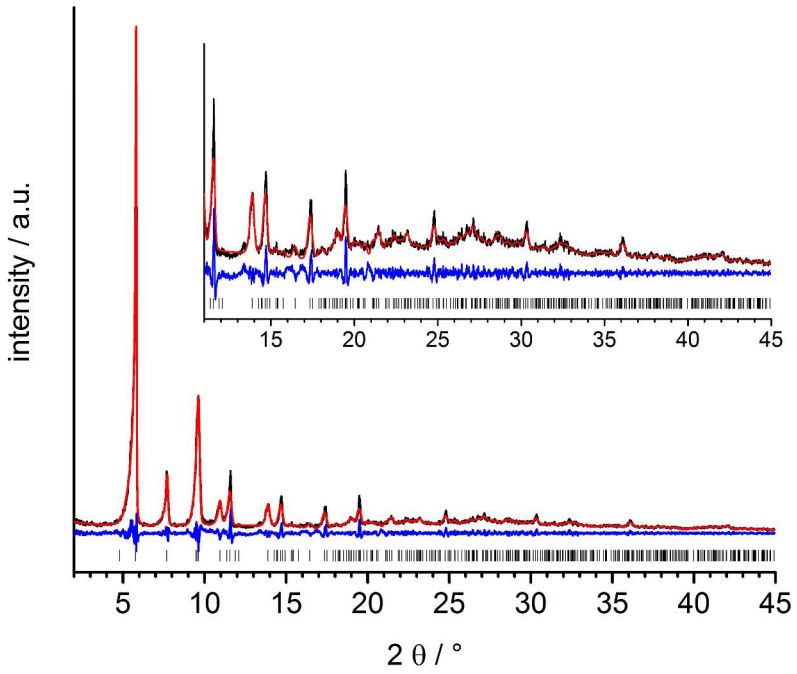

Fig. S14: Le Bail plot of the refinement of *α*-CAU-33. Experimental and theoretical PXRD pattern shown as black and red line, respectively. The difference is drawn in blue, while the positions of the reflections are indicated by black bars.

4. PXRD analyses

The measured and theoretical PXRD patterns of CAU-32 (*as*) are shown in Fig. S15.

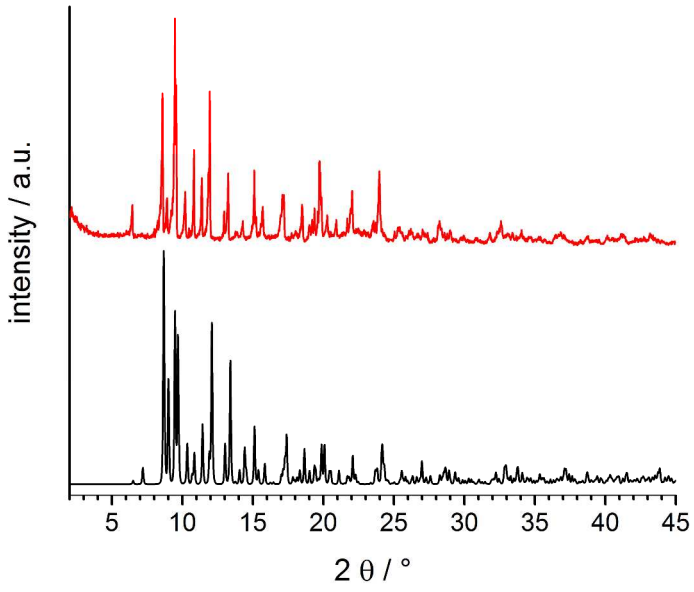

Fig. S15: Measured (top) and theoretical (bottom) PXRD patterns of CAU-32 (*as*).

To get more insight into the structural changes of CAU-32, a fresh sample was synthesized, stored for one day, thermally treated at 60 °C for one day and afterwards washed again with a mixture of MeOH/DMF (4:1). On every step, the sample was characterized by PXRD. The resulting PXRD patterns are shown in Fig. S16. Additionally, the PXRD pattern, which was collected during the T-dependent PXRD experiment at 200 °C (see main article), is given in the figure, as well as a pattern of an activated capillary filled with CAU-32 (activation for one hour at 150 °C at reduced pressure). None of the PXRD patterns could be indexed, which indicates that only mixtures of different structure states are obtained.

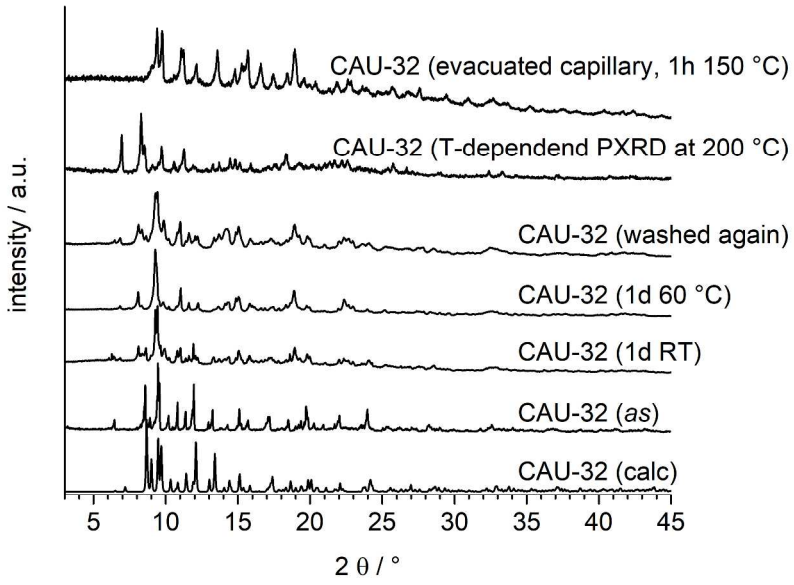

Fig. S16: Theoretical and measured PXRD patterns of CAU-32 upon storage and thermal treatment.

5. Thermogravimetric analyses

The measured TG curves of CAU-31, CAU-32 (*as*) and *β*-CAU-33 are shown in Fig. S17 - Fig. S19. The analyses of the curves are given in the figure captions.

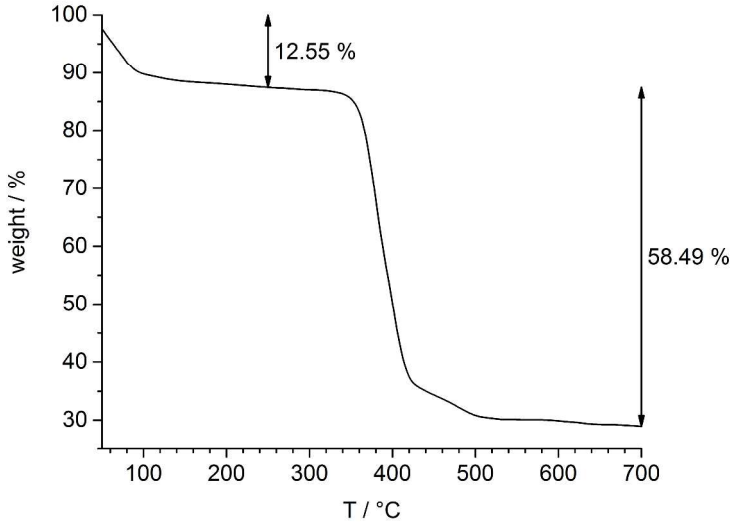

Fig. S17: Measured TG-curve of CAU-31. The measured weight losses match the theoretical values for the loss of water (12.84 %) and decomposition of the linker (60.60 %), calculated using the formula $[Bi_2(O_8C_{34}H_{20})(O_8C_{34}H_{18})(H_2O)_2]\cdot 10.5\ H_2O$. The final product was identified as α-Bi_2O_3.

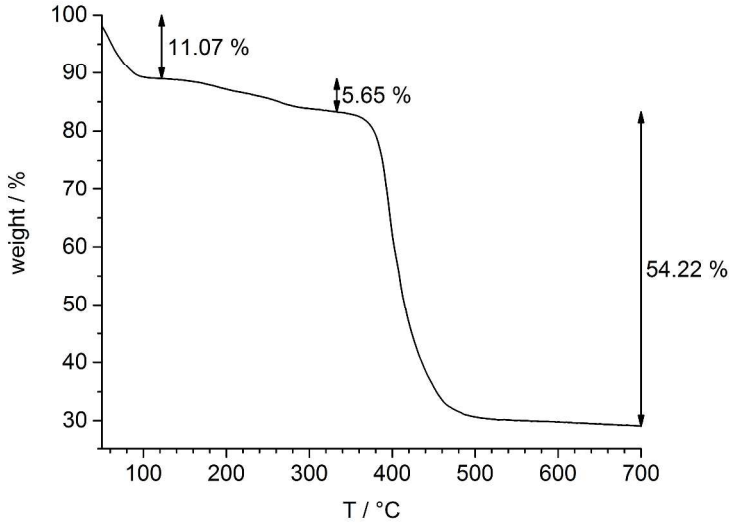

Fig. S18: Measured TG-curve of CAU-32 (*as*). The measured weight losses match the theoretical values for the loss of water (12.01 %), dimethyl ammonium (5.12 %) and decomposition of the linker (58.97 %), calculated using the formula $(NH_2(CH_3)_2)[Bi(O_8C_{34}H_{18})(H_2O)]\cdot 5\ H_2O$. The final product was identified as α-Bi_2O_3.

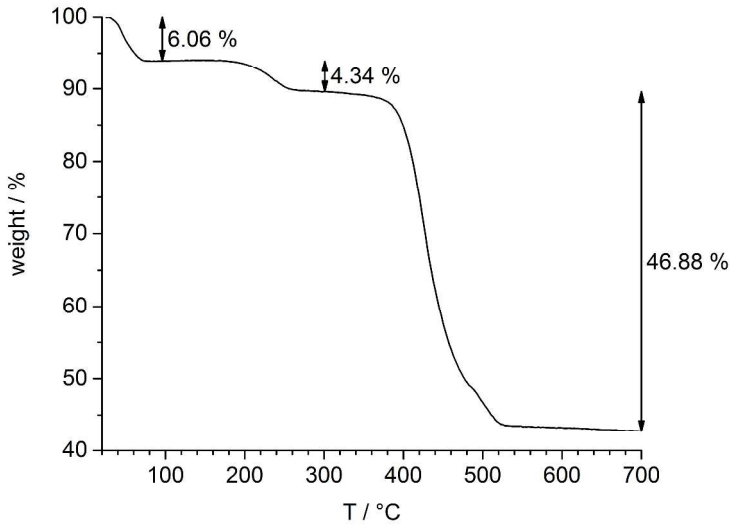

Fig. S19: Measured TG-curve of *β*-CAU-33. The measured weight losses match the theoretical values for the loss of water (6.07 %), DMF (4.56 %) and decomposition of the linker (48.00 %), calculated using the formula $[Bi_4(O)_2(OH)_2(O_8C_{34}H_{20})(O_8C_{34}H_{18})(H_2O)_2]\cdot 5.6\ H_2O\cdot 1.4DMF$. The final product was identified as α-Bi_2O_3.

6. Sorption measurements

The measured isotherms of CAU-31, CAU-32 and CAU-33 are shown in Fig. S20 – Fig. S24. The analyses, measurement parameters as well as the activation procedures are given in the figure captions.

6.1. CAU-31

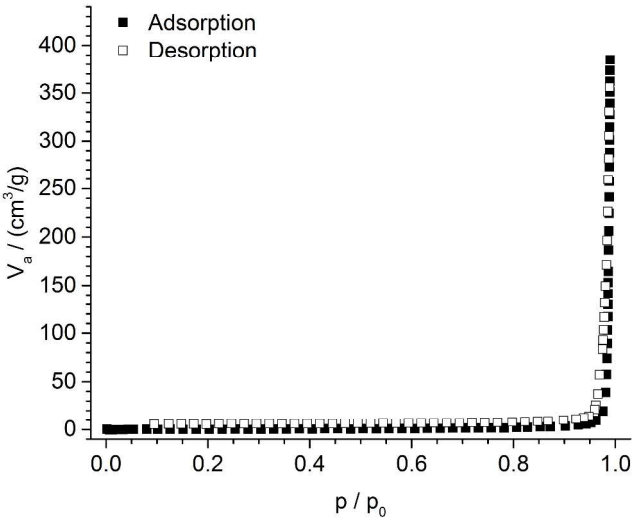

Fig. S20: N_2 sorption isotherm of CAU-31 recorded at 77 K. This graph proves that CAU-31 is not porous towards nitrogen. The sample was activated for 16 h at 100 °C under reduced pressure.

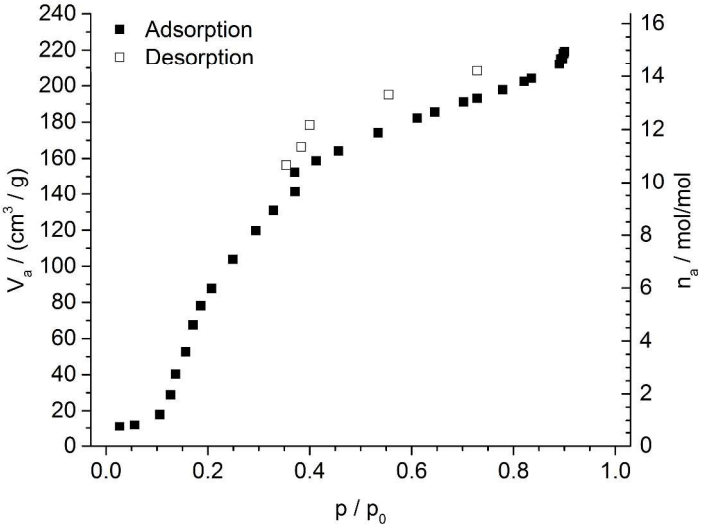

Fig. S21: H_2O sorption isotherm of CAU-31 recorded at 303 K. CAU-31 shows water uptake of 14.95 mol/mol and thus is a porous material. The sample was activated for 16 h at 100 °C under reduced pressure.

6.2. CAU 32

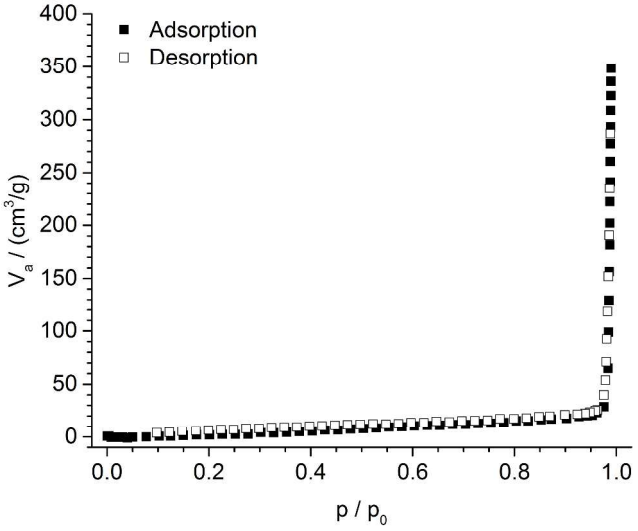

Fig. S22: N_2 sorption isotherm of CAU-32 recorded at 77 K. This graph proves that CAU-32 is not porous towards nitrogen. The sample was activated for 12 h at 150 °C under reduced pressure.

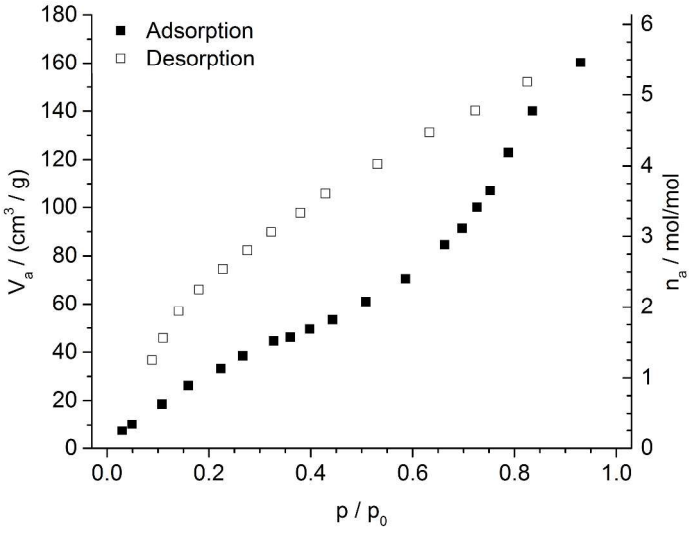

Fig. S23: H_2O sorption isotherm of CAU-32 recorded at 298 K. CAU-32 shows water uptake of 5.46 mol/mol and thus is a porous material. The sample was activated for 12 h at 120 °C under reduced pressure.

6.3. CAU-33

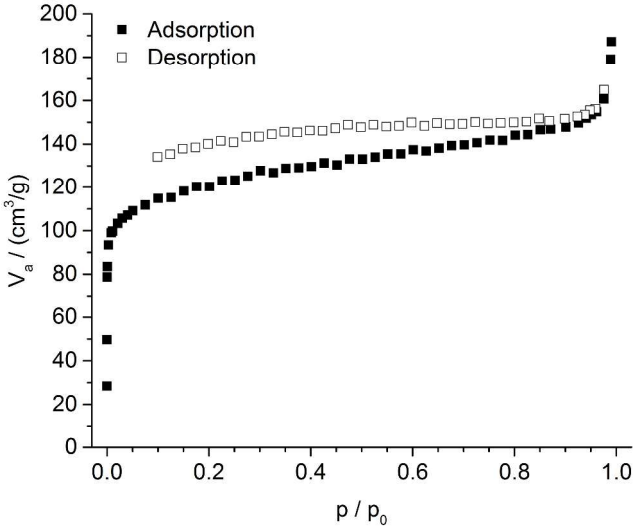

Fig. S24: N_2 sorption isotherm of CAU-33 recorded at 77 K. In this graph a type I(a) isotherm was observed, which confirms the microporosity of the sample. The BET surface area was determined to be a_{BET} = 450 m^2/g and the micropore volume to be V_{mic} = 0.21 cm^3/g. The sample was activated for 12 h at 150 °C under reduced pressure.

7. Infrared spectra

The measured IR spectra of CAU-31, CAU-32 (*as*) and *β*-CAU-33 are shown in Fig. S25 - Fig. S27. The analyses of the characteristic frequencies are given in the figure captions.

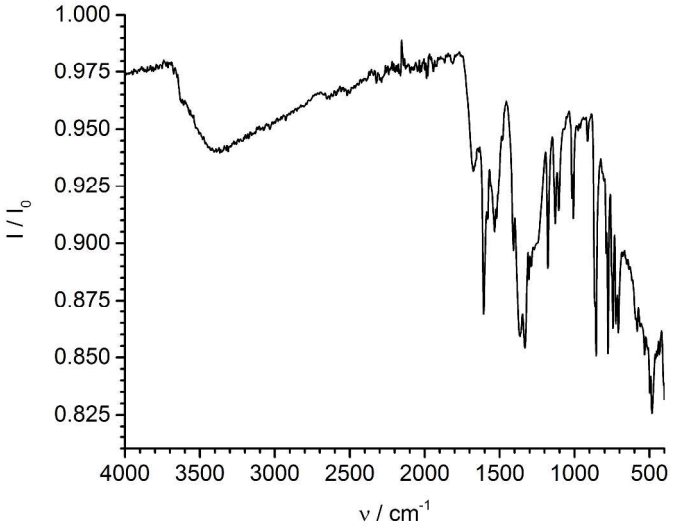

Fig. S25: IR spectrum of CAU-31. Characteristic frequencies: 3700-2700 cm^{-1} (ν(OH), water), 1677 cm^{-1} (ν_{as}(C-O), carboxylate), 1619 cm^{-1}, 1609 cm^{-1} (ν_{s}(C-C), linker), 1534 cm^{-1} (ν_{as}(C-O), carboxylate), 1368 cm^{-1}, 1331 cm^{-1} (ν(OC-OH), carboxylic acid), 1178 cm^{-1},1128 cm^{-1}, 1104 cm^{-1}, 1008 cm^{-1}, 856 cm^{-1}, 777 cm^{-1}, 744 cm^{-1}, 724 cm^{-1}, 707 cm^{-1} (γ(aryl-H), linker).

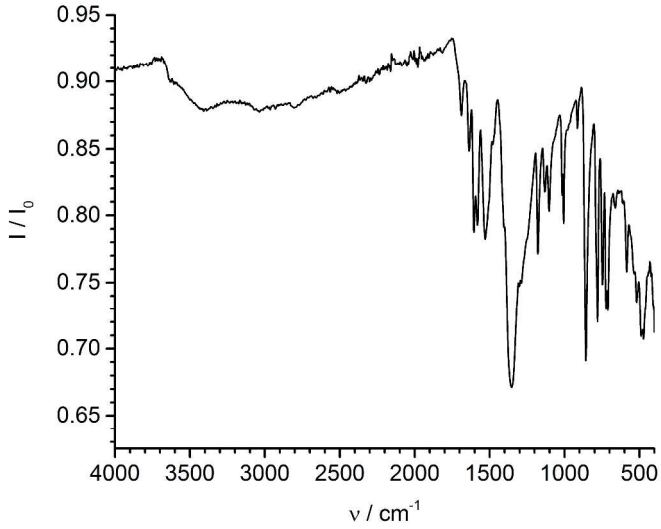

Fig. S26: IR spectrum of CAU-32 (*as*). Characteristic frequencies: 3700-2700 cm^{-1} (ν(OH), water), 3035 cm^{-1}, 2964 cm^{-1}, 2929 cm^{-1}, 2805 cm^{-1}, 2502 cm^{-1} (ν_{as}(N-H), $H_2N(CH_3)_2^+$), 1688 cm^{-1} (ν_{as}(C-O), carboxylate), 1637 cm^{-1}, 1605 cm^{-1} (ν_s(C-C), linker), 1581 cm^{-1} (δ(N-H), $H_2N(CH_3)_2^+$), 1530 cm^{-1} (ν_{as}(C-O), carboxylate), 1352 cm^{-1}, 1287 cm^{-1}, 1301 cm^{-1} (ν(C-N), $H_2N(CH_3)_2^+$), 1178 cm^{-1},1131 cm^{-1}, 1103 cm^{-1}, 1007 cm^{-1} (γ(aryl-H), linker), 914 cm^{-1} (γ(C-H_3), $H_2N(CH_3)_2^+$), 858 cm^{-1}, 780 cm^{-1}, 747 cm^{-1}, 723 cm^{-1}, 710 cm^{-1} (γ(aryl-H), linker).

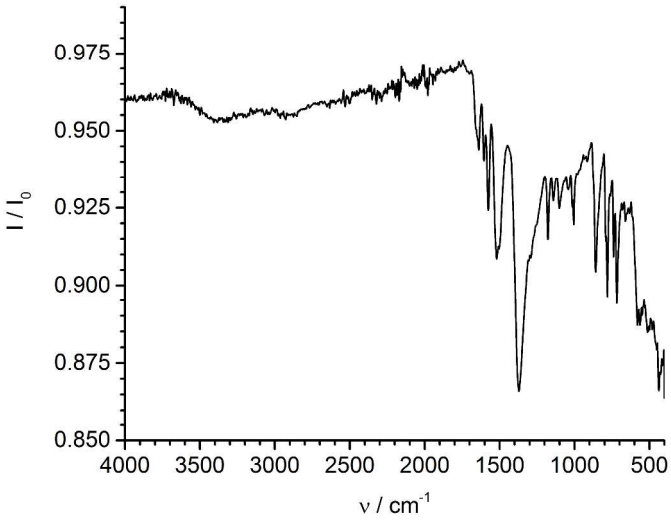

Fig. S27: IR spectrum of CAU-33 (*β*). Characteristic frequencies: 3700-2700 cm^{-1} (ν(OH), water), 1638 cm^{-1}, 1605 cm^{-1} (ν_s(C-C), linker), 1576, 1520 cm^{-1} (ν_{as}(C-O), carboxylate), 1371 cm^{-1} (ν(OC-OH), carboxylic acid), 1178 cm^{-1},1141 cm^{-1}, 1102 cm^{-1}, 1005 cm^{-1}, 859 cm^{-1}, 781 cm^{-1}, 739 cm^{-1}, 717 cm^{-1} (γ(aryl-H), linker). The weak bands between 2500 cm^{-1} and 2000 cm^{-1} are most likely caused by DMF guest molecules.

8. NMR spectroscopy

To confirm that the charge of the anionic network of CAU-32 (*as*) is balanced by $[NH_2(CH_3)_2]^+$ (DMA^+) ions, ^{1}H-NMR spectroscopy was performed on the dissolved sample (Fig. S28).

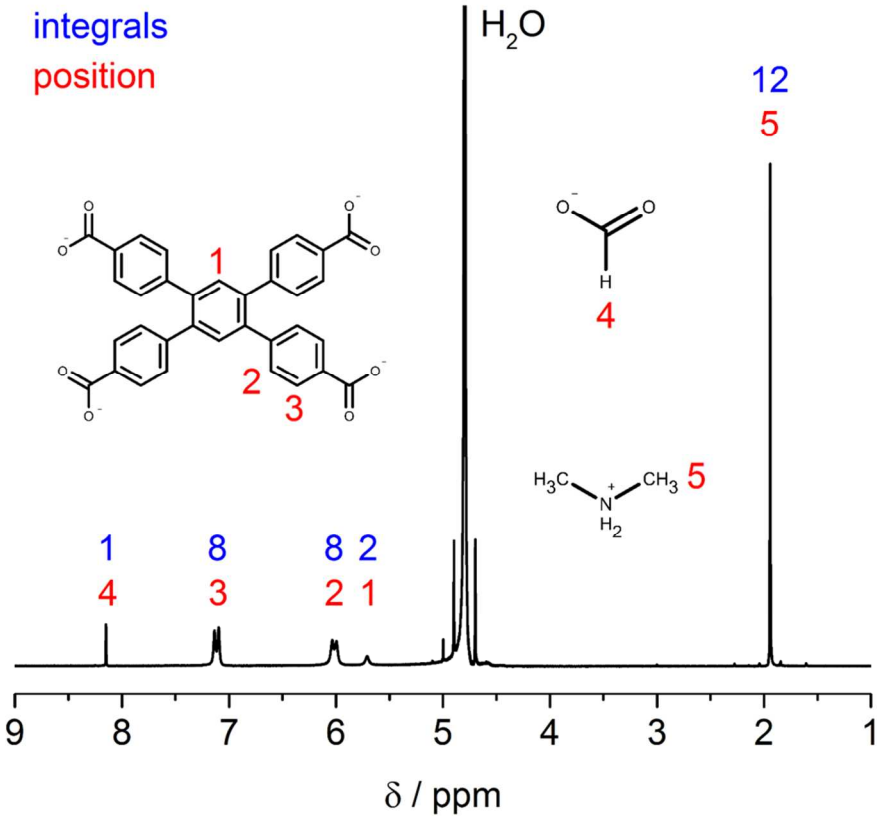

Fig. S28: ^{1}H-NMR spectrum of CAU-32 (*as*) dissolved in 5% NaOD/D_2O. The treatment of DMF with NaOD leads to a decomposition into formate ions and DMA^+ ions. The signal at 8.15 ppm corresponds to 1 formate ion. Since the signal of the CH_3-groups of the DMA^+ ions at 1.94 ppm corresponds to 12 protons, the ratio DMF:DMA^+ was originally 1:1 in the MOF. In addition, the signals of the $TCPB^{4-}$ linker confirm a ratio of DMA^+:$TCPB^{4-}$ of 1:1. This analysis proves that DMA^+ is incorporated in the structure as counter ion. ^{1}H-NMR (200MHz, NaOD/D_2O): δ = 8.15 (1H, s), 7.12 (8H, d), 6.02 (8H, d), 5.70 (2H, s), 1.94 (12H, s) ppm.

9. Chemical stability tests

The PXRD patterns of the samples, after performing the chemical stability experiments with CAU-31, CAU-32 and *β*-CAU-33 are shown in Fig. S29 - Fig. S37. More details on the procedure can be found in the experimental section of the main article.

9.1. CAU-31

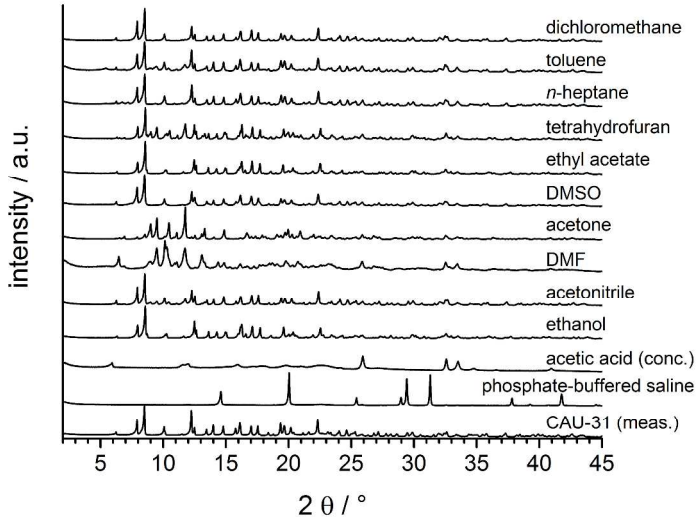

Fig. S29: PXRD patterns of the samples, after performing the chemical stability experiment with CAU-31 in various solvents. The resulting product in phosphate buffered saline was identified as $BiPO_4$.[6] The resulting products in DMF and acetone could not be identified.

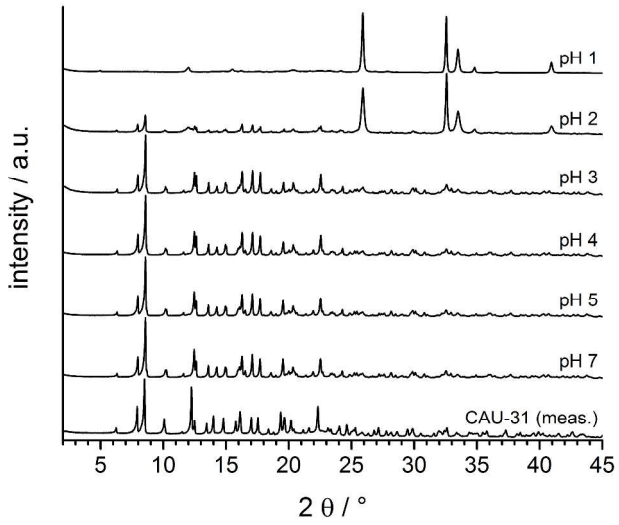

Fig. S30: PXRD patterns of the samples, after performing the chemical stability experiment with CAU-31 in aqueous HCl solutions between pH 1-7. The resulting products at pH 1-2 were identified as BiOCl.[7]

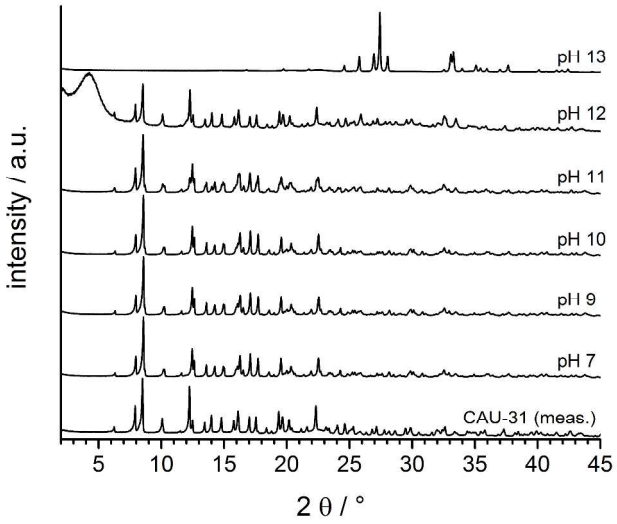

Fig. S31: PXRD patterns of the samples, after performing the chemical stability experiment with CAU-31 in aqueous NaOH solutions between pH 7-13. The resulting product at pH 13 was identified as α-Bi_2O_3.[8]

9.2. CAU-32

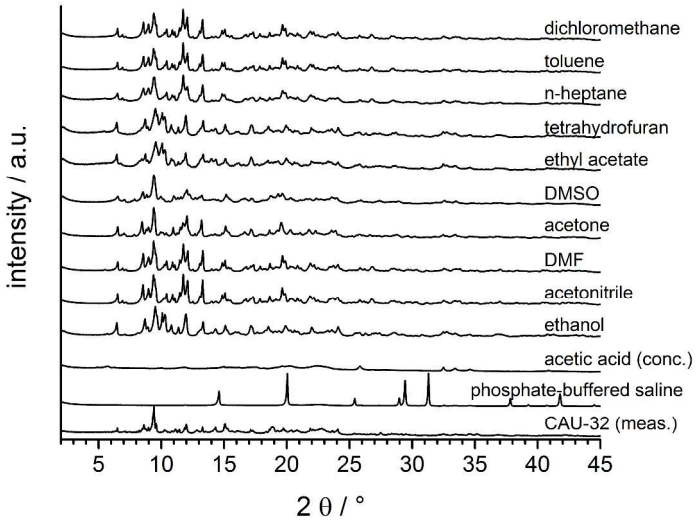

Fig. S32: PXRD patterns of the samples, after performing the chemical stability experiment with CAU-32 in various solvents. The resulting product in phosphate buffered saline was identified as $BiPO_4$.[6] The resulting product in DMSO could not be identified.

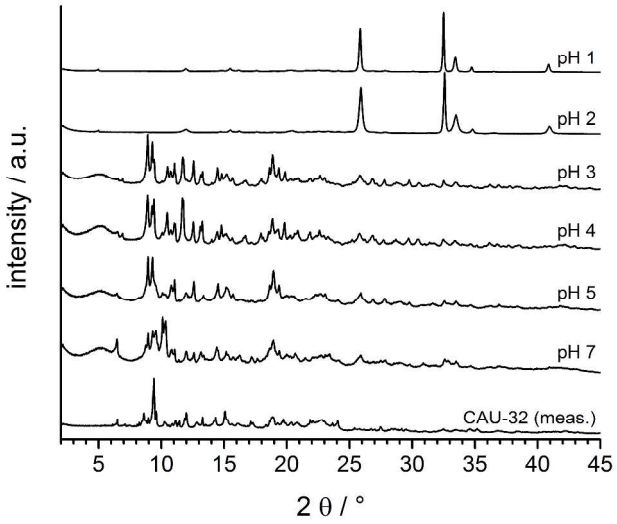

Fig. S33: PXRD patterns of the samples, after performing the chemical stability experiment with CAU-32 in aqueous HCl solutions between pH 1-7. The resulting products at pH 1-2 were identified as BiOCl.[7]

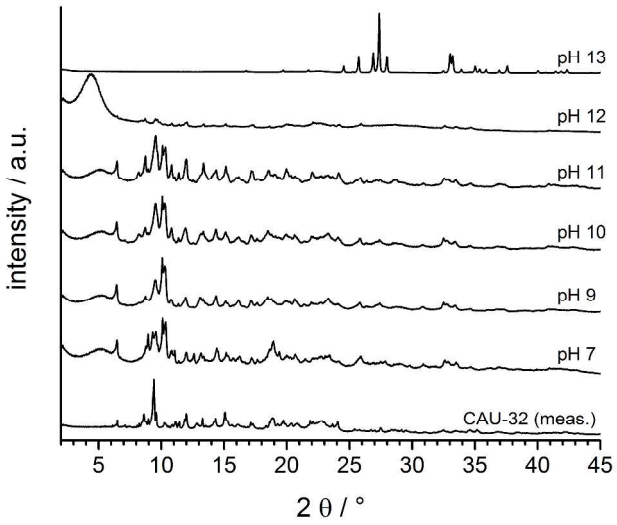

Fig. S34: PXRD patterns of the samples, after performing the chemical stability experiment with CAU-32 in aqueous NaOH solutions between pH 7-13. The resulting product at pH 13 was identified as α-Bi_2O_3.[8]

9.3. CAU-33

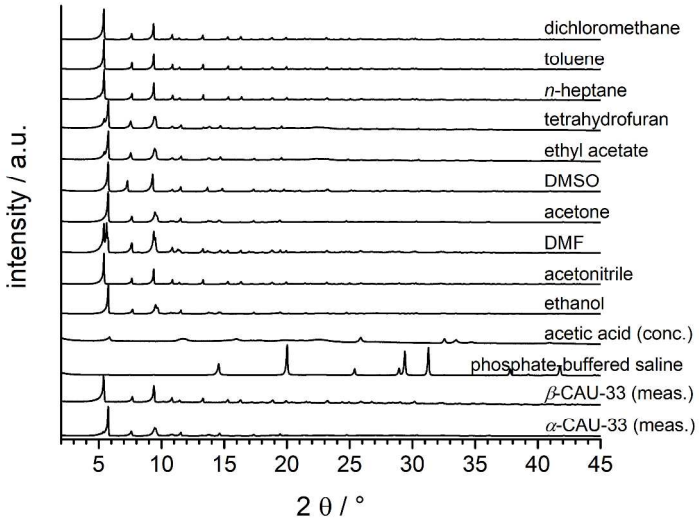

Fig. S35: PXRD patterns of the samples, after performing the chemical stability experiment with *β*-CAU-33 in various solvents. The resulting product in phosphate buffered saline was identified as $BiPO_4$.[6]

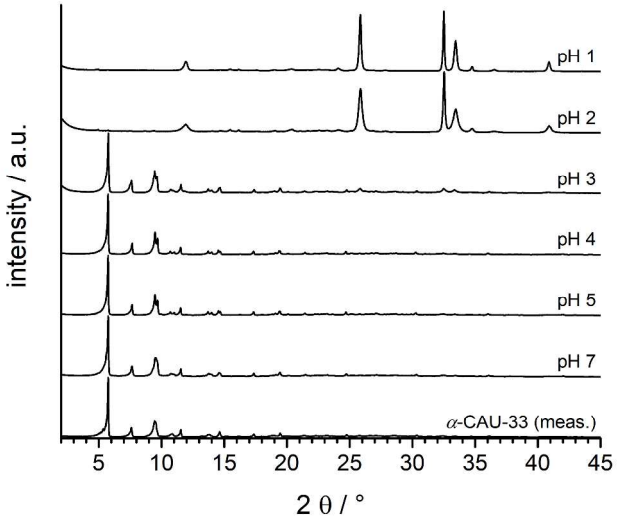

Fig. S36: PXRD patterns of the samples, after performing the chemical stability experiment with *β*-CAU-33 in aqueous HCl solutions between pH 1-7. The resulting products at pH 1-2 were identified as BiOCl.[7]

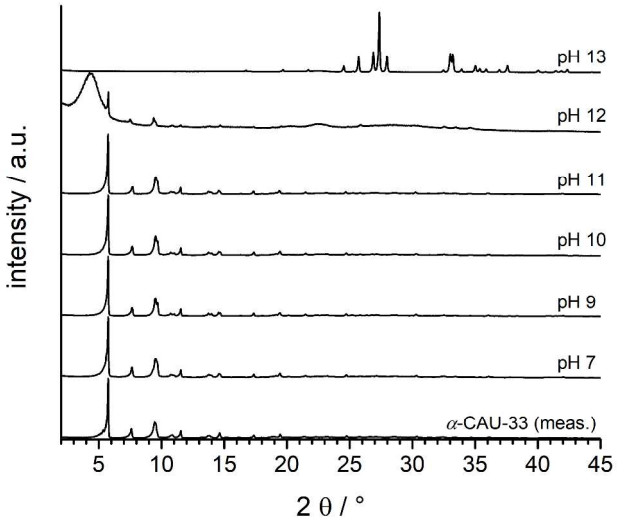

Fig. S37: PXRD patterns of the samples, after performing the chemical stability experiment with *β*-CAU-33 in aqueous NaOH solutions between pH 7-13. The resulting product at pH 13 was identified as α-Bi_2O_3.[8]

10. References

(1) A. Coelho. *TOPAS Academic 6*; Coelho Software, 2016.

(2) Gemmi, M.; La Placa, M. G. I.; Galanis, A. S.; Rauch, E. F.; Nicolopoulos, S. Fast electron diffraction tomography. *J. Appl. Crystallogr.* **2015**, *48*, 718–727.

(3) Wan, W.; Sun, J.; Su, J.; Hovmöller, S.; Zou, X. Three-dimensional rotation electron diffraction: Software RED for automated data collection and data processing. *J. Appl. Crystallogr.* **2013**, *46*, 1863–1873.

(4) Kabsch, W. Integration, scaling, space-group assignment and post-refinement. *Acta Crystallogr., Sect. D: Biol. Crystallogr.* **2010**, *66*, 133–144.

(5) Sheldrick, G. M. SHELXT - integrated space-group and crystal-structure determination. *Acta Crystallogr., Sect. A: Found. Adv.* **2015**, *71*, 3–8.

(6) PDF database. bismuth phosphate, [15-766].

(7) Keramidas, K. G.; Voutsas, G. P.; Rentzeperis, P. I. The crystal structure of BiOCl. *Z. Kristallogr. - Cryst. Mater.* **1993**, *205,* DOI: 10.1524/zkri.1993.205.12.35.

(8) Sillén, L. G. Die Kristallstruktur des monoklinen α-Bi2O3. *Naturwissenschaften* **1940**, *28*, 206–207.